JCTC Journal of Chemical Theory and Computation

Article

pubs.acs.org/JCTC

Ewald Summation for Molecular Simulations

Brad A. Wells* and Alan L. Chaffee*

Cooperative Research Centre for Greenhouse Gas Technologies (CO2CRC), School of Chemistry, Monash University, Melbourne, VIC 3800, Australia

Supporting Information

ABSTRACT: Ewald summation is an important technique for molecular simulation. In this article, expressions are provided for implementing Ewald summation for any inverse power potential in a range of different simulations. Energies, forces, stresses, and Hessian elements as well as truncation errors are considered. Focus is also given to methods for accelerating Ewald summation in Monte Carlo simulations, particularly in the grand canonical ensemble. Ewald techniques are applied to the simulation of CO_2 adsorption and diffusion in the metal−organic framework, MOF-5. These simulations show that optimized Ewald summation can provide increased accuracy at similar computational cost compared to that of pair-based methods.

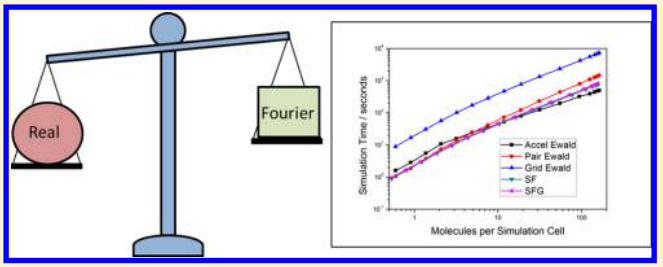

1. INTRODUCTION

Molecular simulation using empirically derived potentials has arisen as a useful tool for gaining insight into a wide range of problems. Many different types of simulations, including Monte Carlo[1] and molecular dynamics,[2] in a range of thermodynamic ensembles have been created to address problems spanning the breadth of the chemical sciences. As just one example, grand canonical Monte Carlo (GCMC) simulation is a widely used and important tool for understanding gas adsorption, separation, and storage in many different classes of porous materials.[3] This has a wide range of applications, including areas such as hydrogen storage[4] and carbon dioxide capture.[5]

While some types of simulations use intramolecular potentials to represent bond stretching, bending, and twisting potentials, nearly all molecular simulations include an account of nonbonding interactions. For most simulations, these interactions extend beyond the coordination sphere of each atom, and their calculation comprises the majority of the computational effort required.[6] Optimizing the calculation of these interactions, therefore, is essential for large-scale applications of molecular simulation. One example of such large-scale simulation is the application of GCMC simulations to scanning the gas adsorption properties of experimental and hypothetical databases of porous materials.[7]

Usually, nonbonding interactions are divided into dispersion, repulsion, and electrostatic contributions. These potentials are usually represented using reciprocal distance potentials, as shown in eq 1

$$U(r) = \frac{A_{\text{rep}}}{r^{12}} - \frac{B_{\text{disp}}}{r^{6}} + \frac{q_1 q_2}{4\pi\epsilon_0 r} \tag{1}$$

In the case of the dispersion and repulsion parameters, the potential scale factors A_{rep} and B_{disp} are normally considered to be transferable between atoms in similar chemical environments and thus a number of standard force fields have been created for a large range of atom types.[8] The atomic charges q_n are not as transferable, and for many materials, accurate simulation requires the explicit calculation of charges.[9] The development of appropriate methods for assigning charges for molecular simulation remains an active area of research.[10]

One of the main challenges in calculating these potentials in periodic systems is their generally slow convergence with distance. Because these potentials are defined $\forall r \geq 0$ and closed forms of the sums are not known, they must be truncated at some cutoff distance to be practically evaluated. Contributions beyond this cutoff distance are generally ignored, introducing systematic errors to the calculation.[11] One of the most problematic cutoff errors is that introduced for Coulombic or other slowly decaying potentials. Here, the tail, U_{tail}, of the potential $U_n(r) = B/r^n$ beyond a cutoff distance r_c in a system of N particles with uniform density ρ is given as[12]

$$U_{\text{tail}} = 2\pi N\rho \int_{r_c}^{\infty} U_n(r) r^2 \, \mathrm{d}r = 2\pi N\rho \int_{r_c}^{\infty} \frac{B r^2}{r^n} \, \mathrm{d}r \tag{2}$$

The infinite value of this tail for $n \leq 3$ indicates that the potential sum of a uniformly distributed set of points is nonconvergent. Therefore, potentials where $n \leq 3$ are only conditionally convergent where the pattern of point interactions are sufficiently sparse and nonuniform to allow convergence of the potential.

One of the main approaches to deal with this problem is that of Ewald summation. This method was first developed for systems of three-dimensional periodic electrostatic monop-

Received: February 1, 2015
Published: July 22, 2015

DOI: 10.1021/acs.jctc.5b00093
J. Chem. Theory Comput. 2015, 11, 3684−3695

oles,[13] but it has subsequently also been applied to dispersion potentials,[14] higher order electrostatic multipoles,[15] and systems of one or two dimensions of periodicity.[16] The main insight of this method is that, using a convergence function and a Fourier transform, a single conditionally or slowly convergent sum can be transformed into two rapidly convergent sums. Due to their rapid convergence, these sums can be evaluated to high accuracy, thereby avoiding the computational artifacts introduced by more approximate cutoff-based methods.

Building on the base equations, several different types of inter-related mesh-based Ewald schemes have been created that are suited to some types of simulations.[17] These include the particle mesh Ewald (PME) method,[18] the smoothed particle mesh Ewald (SPME) method,[19] particle particle particle mesh (PPPM) method,[20] and the fast Fourier Poisson (FFP) method.[21] While Ewald summation can, in theory, be used for any inverse distance potential, many descriptions of the FFT Ewald summation have considered only electrostatic interactions, although London dispersion is beginning to be considered.[22] Because each of these methods relies on the fast Fourier transform (FFT) of a three-dimensional grid, they are well-suited to simulations, such as typical molecular dynamics, where the entire system is perturbed at each step.

The main drawback to Ewald summation is that this technique scales between $O(N^{3/2})$ and $O(N^2)$ for the direct algorithms[12,23] and $O(N \log N)$ for the FFT algorithms,[18] where N is the number of atoms in the simulation. This is larger than the $O(N)$ scaling typical for large simulations with truncated pairwise potentials, resulting in significantly more computational effort being required. To address this problem, a number of pairwise potential methods have been suggested, mostly for electrostatic interactions.[24] These have included potentials based on reaction fields,[25] charge neutralization,[26] shifted forces,[27] distance-dependent dielectrics,[11] isotropic periodic sums,[28] and truncated Ewald sums.[29] While these potentials allow for rapid calculation of the potential interactions, the errors associated with each approach are difficult to predict. This problem is particularly acute for electrostatic potentials due to their conditional convergence. For instance, studies have shown that cutoff-based potentials can lead to inaccuracies in calculating properties such as heat of adsorption,[30] internal energy, pressure,[31] and surface tension.[22a] Other recent work has also shown that the computational effort required for properly converged electrostatic pairwise interactions is similar to that for optimized Ewald summation.[32]

The different types of treatments for long-range nonbonding interactions are suited to different types of simulations. In some types of molecular simulation, such as in Monte Carlo-based methods, only a relatively small number of atoms are moved between energy evaluations. Here, the simple direct Ewald methods are most efficient, as the FFT methods are hindered by the requirement to recalculate the whole grid for only a small number of interactions. Simulations of this type also present some opportunities for optimizing the efficiency of Ewald summations based on intelligent selection of summation parameters and the storage and reuse of large parts of the reciprocal space sum. These optimizations can help to provide significant improvements to the speed of the calculation by effectively reusing previous energy evaluations.

In this article, we show how Ewald summation can be used for any inverse distance potential to an integer power. The necessary formulas for calculating molecular energies, forces, stresses, and Hessian matrix elements are derived. Formulas for estimating appropriate convergence parameters and cutoffs are also discussed. A discussion of how Ewald techniques can be optimized for Monte Carlo simulation is also provided, with particular focus on GCMC and equilibrium molecular dynamics (EMD) simulations. We then apply these techniques to the simulation of CO_2 adsorption and diffusion in the metal−organic framework (MOF), MOF-5 or IRMOF-1.

2. EWALD FORMULAS

2.1. Energies. The general idea underlying Ewald summation is to decompose the original sum of terms into two separate sums using a convergence function $\phi(r)$ such that the energy U_n from a given potential can be given as

$$U_n = \frac{1}{2}\sum_{\boldsymbol{l}}\sum_{ij}^{N}\frac{B_{ij}}{|\boldsymbol{r}_{ij}+\boldsymbol{l}|^n} = \frac{1}{2}\sum_{\boldsymbol{l}}\sum_{ij}^{N}\frac{B_{ij}\phi(r_{ij})}{|\boldsymbol{r}_{ij}+\boldsymbol{l}|^n} + \frac{1}{2}\sum_{\boldsymbol{l}}\sum_{ij}^{N}\frac{B_{ij}[1-\phi(r_{ij})]}{|\boldsymbol{r}_{ij}+\boldsymbol{l}|^n} \quad (3)$$

Here, n represents the power of the potential, and the sum of terms is carried out both over the minimum atomic distances $\boldsymbol{r}_{ij}$ as well as the lattice vectors $\boldsymbol{l}$. While the first sum can be evaluated directly, the second sum, which contains the long-range tail, is evaluated through a Fourier transform. The values of the convergence function should be both smooth for low values of r_{ij} and rapidly decay to 0 for high values of r_{ij}. This ensures both the rapid convergence of the first sum and allows for the second sum to be accurately represented with a small number of plane waves. Following Nijboer and de Wette[33] as well as Williams,[14c] we use the convergence function

$$\phi(r) = \frac{\Gamma\left(\frac{n}{2}, \alpha^2 r^2\right)}{\Gamma\left(\frac{n}{2}\right)} \quad (4)$$

Here, α is a convergence parameter that controls the size of each sum and $\Gamma(n,x)$ represents the upper incomplete gamma function, given as

$$\Gamma(n,x) = \int_x^\infty t^{n-1}\,\mathrm{e}^{-t}\,\mathrm{d}t = 2\int_{\sqrt{x}}^\infty u^{2n-1}\,\mathrm{e}^{-u^2}\mathrm{d}u \quad (5)$$

This can be easily evaluated for any required half integer value of n using the recurrence relationship

$$\Gamma(n,x) = (n-1)\Gamma(n-1,x) + x^{n-1}\,\mathrm{e}^{-x} \quad (6)$$

and the values

$$\Gamma(1,x) = \mathrm{e}^{-x}$$
$$\Gamma\left(\frac{1}{2}, x\right) = \sqrt{\pi}\,\mathrm{erfc}(\sqrt{x}) \quad (7)$$

Splitting the total energy U_n into its real space, reciprocal space, and self-correction components U_n^r, U_n^f, and U_n^0, respectively, leads to the general expression for the energy U_n

DOI: 10.1021/acs.jctc.5b00093
J. Chem. Theory Comput. 2015, 11, 3684−3695

$$U_n = U_n^r + U_n^f + U_n^0$$

$$U_n^r = \frac{1}{2\Gamma\left(\frac{n}{2}\right)} \sum_{\boldsymbol{l}}^{*} \sum_{ij} \frac{B_{ij}\Gamma\left(\frac{n}{2}, a^2\right)}{|\boldsymbol{r}_{ij} + \boldsymbol{l}|^n}$$

$$U_n^f = \frac{\pi^{3/2}}{2^{n-2}\Gamma\left(\frac{n}{2}\right)V} \sum_{\boldsymbol{k}\neq 0} |\boldsymbol{k}|^{n-3}\Gamma\left(\frac{3-n}{2}, b^2\right)\left[\sum_{ij} B_{ij}\cos(\boldsymbol{k}\cdot\boldsymbol{r}_{ij})\right]$$

$$U_n^0 = \frac{\pi^{3/2}\alpha^{n-3}}{(n-3)V\Gamma\left(\frac{n}{2}\right)}\left[\sum_{ij} B_{ij}\right] - \frac{\alpha^n}{n\Gamma\left(\frac{n}{2}\right)}\left[\sum_{i} B_{ii}\right] \tag{8}$$

A full derivation of these formulas is given in the Supporting Information. Here, the asterisk (*) in the real space summation indicates that the $|\boldsymbol{r}_{ij} + \boldsymbol{l}| = 0$ terms are ignored, V is the volume of the unit cell, $a = \alpha|\boldsymbol{r}_{ij} + \boldsymbol{l}|$, $b = |\boldsymbol{k}|/2\alpha$, and the reciprocal vectors $\boldsymbol{k}$ are given as combinations of the reciprocal cell unit vectors $\boldsymbol{k}_u$, where

$$\boldsymbol{k}_u = 2\pi\frac{\boldsymbol{l}_v \times \boldsymbol{l}_w}{V} \tag{9}$$

Here, u, v, and w are the indices for the three lattice vectors. These formulas for Ewald energies are similar to those given by Williams,[14c] with the difference being the placement of factors of 2π in the reciprocal vectors and $\pi^{1/2}$ in the value of α.

A number of simplifications may be made as to how the reciprocal space energy sum is calculated. First, it can be noted that because of the simple trigonometric identity

$$\cos(\boldsymbol{k}\cdot\boldsymbol{r}_{ij}) + \cos(-\boldsymbol{k}\cdot\boldsymbol{r}_{ij}) = 2\cos(\boldsymbol{k}\cdot\boldsymbol{r}_{ij}) \tag{10}$$

only half of the possible k-vectors for a given cutoff need to be evaluated. Second, another optimization is possible in cases where the unit cell vectors, and thus the reciprocal vectors, are orthogonal. Here, the zero components of the reciprocal vectors produced by each being aligned to the coordinate system allow the reduction of the sum over reciprocal vectors

$$\sum_{n_u=-N_u}^{N_u*}\sum_{n_v=-N_v}^{N_v}\sum_{n_w=-N_w}^{N_w} \cos([n_u\boldsymbol{k}_u + n_v\boldsymbol{k}_v + n_w\boldsymbol{k}_w]\cdot\boldsymbol{r}_{ij}) = \sum_{n_u=0}^{N_u*}\sum_{n_v=0}^{N_v}\sum_{n_w=0}^{N_w} \mathrm{H}(n_u,n_v,n_w)\cos(n_u k_u^x r_{ij}^x)\cos(n_v k_v^y r_{ij}^y)\cos(n_w k_w^z r_{ij}^z) \tag{11}$$

Here, the asterisk in the summation over n_u indicates that the $n_u = n_v = n_w = 0$ term, which corresponds to $\boldsymbol{k} = 0$, is ignored. The function H gives the correct factor for each term and can be given as

$$\mathrm{H}(n_u,n_v,n_w) = [2 - \delta(n_u)][2 - \delta(n_v)][2 - \delta(n_w)] \tag{12}$$

Here, δ represents the Dirac delta function. This cancellation reduces the number of reciprocal vectors that need to be evaluated by roughly a factor of 8. Additionally, it also reduces the number of necessary evaluations of the cosine function. As each component of the total reciprocal vector is independent of the others, it is possible to evaluate and store the cosine function evaluations for each component. These stored cosine values can then be combined through multiplication for each reciprocal vector considered. For cubic unit cells where $k_u^x = k_v^y = k_w^z$, the minimum number of cosine evaluations can be further reduced by a factor of 3. As these methods can be applied only to cubic, tetragonal, or orthorhombic unit cells, a trade-off here needs to be made between computational efficiency and program generality or complexity. The utility of these optimizations, therefore, depends on the prevalence of orthogonal unit cells in the specific problem space being studied.

These reciprocal space sums assume nothing of the nature of the potential coefficient B_{ij}. There are, however, some important optimizations that may be made depending on how B_{ij} is defined. In the case where B_{ij} is defined by the geometric combination rule

$$B_{ij} = \sqrt{B_{ii} \times B_{jj}} \tag{13}$$

then the structure factor term in the expression for the reciprocal energy can be transformed into two one-dimensional sums such that

$$\sum_{ij} B_{ij}\cos(\boldsymbol{k}\cdot\boldsymbol{r}_{ij}) = \left[\sum_i \sqrt{B_{ii}}\cos(\boldsymbol{k}\cdot\boldsymbol{r}_i)\right]^2 + \left[\sum_i \sqrt{B_{ii}}\sin(\boldsymbol{k}\cdot\boldsymbol{r}_i)\right]^2 \tag{14}$$

Alternatively, this sum can be written using structure factors $S(\boldsymbol{k})$ such that

$$\sum_{ij} B_{ij}\cos(\boldsymbol{k}\cdot\boldsymbol{r}_{ij}) = \left[\sum_j \sqrt{B_{jj}}\, e^{i\boldsymbol{k}\cdot\boldsymbol{r}_j}\right]\left[\sum_j \sqrt{B_{jj}}\, e^{-i\boldsymbol{k}\cdot\boldsymbol{r}_j}\right] = S(\boldsymbol{k})S(-\boldsymbol{k}) \tag{15}$$

This changes the scaling of the computational effort in calculating reciprocal term to scaling linearly with the number of atom in the system. Force fields such as the DREIDING[8c] and OPLS-AA[8b] use this combination rule for both dispersion and repulsion potentials, whereas others such as the COMPASS[34] force field uses this combination rule for dispersion interactions only.

In cases where there is no geometric relationship between the single atom parameters B_{ii} and the pairwise parameters B_{ij}, it can still be more efficient computationally to group atoms of the same atom force field type into sets I and J.[14a] This enables the transformation of the structure factor

$$\sum_{ij} B_{ij}\cos(\boldsymbol{k}\cdot\boldsymbol{r}_{ij}) = \frac{1}{2}\sum_{IJ} B_{IJ}\sum_{i\in I}\sum_{j\in J}\left[e^{i\boldsymbol{k}\cdot\boldsymbol{r}_{ij}} + e^{-i\boldsymbol{k}\cdot\boldsymbol{r}_{ij}}\right] = \sum_{IJ} B_{IJ}\left[\sum_{i\in I} e^{i\boldsymbol{k}\cdot\boldsymbol{r}_i}\right]\left[\sum_{j\in J} e^{-i\boldsymbol{k}\cdot\boldsymbol{r}_j}\right] \tag{16}$$

Assuming that each atom type sum can be stored, this expression also scales linearly with the number of atoms in the system. Since most systems have a relatively small number of atom types, this represents a large savings in computational effort. This scheme can be used with force fields that use arithmetic or Lorentz−Berthelot combination rules such as the Universal[35] and TraPPE[36] force fields.

Using these formulas, it is possible to derive the Ewald summation of any r_{ij}^{-n} potential where $n > 3$ or where $\sum_{ij} B_{ij} = 0$. For instance, setting $n = 1$ and $n = 6$ obtains the expressions for the Coulombic and London dispersion energies given by Karasawa and co-workers.[14b]

2.2. Forces. Forces on atoms and stresses on the periodic cell of a material are critical quantities for a range of simulations including EMD and molecular structure optimization. Some

DOI: 10.1021/acs.jctc.5b00093
J. Chem. Theory Comput. 2015, 11, 3684−3695

biased Monte Carlo moves, such as the force-bias Monte Carlo method, also make use of atomic forces.[37] Forces are simply calculated by taking the derivative of the energy with respect to the interatomic distance r_{ij}, using the identity

$$\boldsymbol{f}_i = -\frac{\partial U(\boldsymbol{r})}{\partial \boldsymbol{r}_i} = -\sum_j \hat{r}_{ij}\frac{\partial U(\boldsymbol{r})}{\partial r_{ij}} \tag{17}$$

This produces forces on the ith atom for a r_{ij}^{-n} potential $\boldsymbol{f}_{i,n}$ where

$$\begin{aligned}
&\boldsymbol{f}_{i,n} = \boldsymbol{f}^r_{i,n} + \boldsymbol{f}^f_{i,n}\\
&\boldsymbol{f}^r_{i,n} = \frac{\alpha^{n+1}}{\Gamma\left(\frac{n}{2}\right)}\sum_{\boldsymbol{l}}^{*}\sum_j B_{ij}(\widehat{\boldsymbol{r}_{ij}+\boldsymbol{l}})\left\{\frac{2e^{-a^2}}{a} + \frac{n\Gamma\left(\frac{n}{2},a^2\right)}{a^{n+1}}\right\}\\
&\boldsymbol{f}^f_{i,n} = \frac{\pi^{\frac{3}{2}}}{2^{n-3}\Gamma\left(\frac{n}{2}\right)V}\sum_{\boldsymbol{k}\neq\boldsymbol{0}}\boldsymbol{k}|\boldsymbol{k}|^{n-3}\Gamma\left(\frac{3-n}{2},b^2\right)\left[\sum_j B_{ij}\sin(\boldsymbol{k}\cdot\boldsymbol{r}_{ij})\right]
\end{aligned} \tag{18}$$

Assuming that the pairwise potential coefficient can be written as a product of single potential coefficients allows the reciprocal-based atomic force to be written using structure factors such that

$$\boldsymbol{f}^f_{i,n} = \frac{\pi^{3/2}}{2^{n-2}\Gamma\left(\frac{n}{2}\right)V}\sum_{\boldsymbol{k}\neq 0}\sqrt{B_{ii}}\boldsymbol{k}\,|\boldsymbol{k}|^{n-3}\Gamma\left(\frac{3-n}{2},b^2\right)\left(i\,e^{-i\boldsymbol{k}\cdot\boldsymbol{r}_i}S(\boldsymbol{k}) - i\,e^{i\boldsymbol{k}\cdot\boldsymbol{r}_i}S(-\boldsymbol{k})\right) \tag{19}$$

This again reduces the two-dimensional sum over atom pairs to two single-dimensional sums over atoms.

2.3. Stress. The stress tensor $\boldsymbol{\Pi}$ is used in simulations that vary the size or shape of the unit cell. Examples of such simulations include geometry optimizations that include the unit cell vectors or EMD simulations in either the NPT or NPH ensemble. Stress is also necessary in Monte Carlo simulations in the osmotic ensemble.[38]

The stress tensor is defined by the relationship[14b]

$$-\frac{\partial U}{\partial \boldsymbol{L}_{\alpha\gamma}} = \sum_\beta \boldsymbol{\Pi}_{\alpha\beta}V\boldsymbol{L}^{-1}_{\gamma\beta} \tag{20}$$

Here, $\boldsymbol{L}$ represents the tensor formed from the three unit cell vectors. In cases where the interatomic potential does not depend on the unit cell volume, as in the case of the real space sum, the stress is simply given by the relationship

$$\boldsymbol{\Pi} = \sum_{ij}\boldsymbol{f}_{ij}\otimes\boldsymbol{r}_{ij} \tag{21}$$

Here, $\otimes$ represents the tensor product. Thus, the stress contribution from the real space forces is given as

$$\boldsymbol{\Pi}^r = \frac{\alpha^{n+1}}{\Gamma\left(\frac{n}{2}\right)}\sum_{\boldsymbol{l}}^{*}\sum_{ij}B_{ij}(\widehat{\boldsymbol{r}_{ij}+\boldsymbol{l}})\otimes(\boldsymbol{r}_{ij}+\boldsymbol{l})\left\{\frac{2e^{-a^2}}{a} + \frac{n\Gamma\left(\frac{n}{2},a^2\right)}{a^{n+1}}\right\} \tag{22}$$

while the reciprocal space stress is given as

$$\boldsymbol{\Pi}^f = \frac{\pi^{3/2}2^{2-n}}{\Gamma\left(\frac{n}{2}\right)V}\sum_{\boldsymbol{k}\neq 0}\left\{\sum_{ij}B_{ij}\cos(\boldsymbol{k}\cdot\boldsymbol{r}_{ij})\left[\frac{\Gamma\left(\frac{3-n}{2},b^2\right)}{|\boldsymbol{k}|^{3-n}}\boldsymbol{I} - \frac{2\Gamma\left(\frac{5-n}{2},b^2\right)}{|\boldsymbol{k}|^{5-n}}\boldsymbol{k}\otimes\boldsymbol{k}\right]\right\} \tag{23}$$

Similar to the reciprocal energy expression, the structure factor part of this expression can be replaced with one-dimensional sums to make the evaluation of this term more efficient.

There is also a contribution to the stress that arises from the $\boldsymbol{k} = 0$ term, which is a consequence of this contribution to the total energy being dependent on the unit cell volume. This stress component is given as

$$\boldsymbol{\Pi}^0 = \frac{\pi^{3/2}\alpha^{n-3}}{(n-3)V\Gamma\left(\frac{n}{2}\right)}\left[\sum_{ij}B_{ij}\right]\boldsymbol{I} \tag{24}$$

Here, $\boldsymbol{I}$ represents the identity tensor. In systems with an electrostatically neutral unit cell, this term is zero for the Coulomb potential, as it includes the sum of the atomic charges.

2.4. Hessian. The Hessian or second-derivative matrix elements H are used in a range of simulations for calculating properties such as phonons and also in geometry optimization. Hessian elements can be written as $H^{\mu\nu}_{ij}$, representing the Cartesian components μ and ν of the second derivatives from atoms i and j. Hessian elements where the two derivatives are taken on the same atom, $H^{\mu\nu}_{ii}$, can be given as

$$\begin{aligned}
H^{\mu\nu}_{ii} &= \sum_j \frac{\partial^2 U_{ij}(\boldsymbol{r})}{\partial r^\mu_i \partial r^\nu_i}\\
&= \sum_j\left(\frac{\delta_{\mu\nu}}{r_{ij}} - \frac{r^\mu_{ij}r^\nu_{ij}}{r^3_{ij}}\right)\frac{\partial U_{ij}(\boldsymbol{r})}{\partial r_{ij}} + \frac{r^\mu_{ij}r^\nu_{ij}}{r^2_{ij}}\frac{\partial^2 U_{ij}(\boldsymbol{r})}{\partial r^2_{ij}}
\end{aligned} \tag{25}$$

Here, $U_{ij}(\boldsymbol{r})$ represents the energy from the interaction of atoms i and j. In the case where derivatives are taken on different atoms, then

$$H^{\mu\nu}_{ij} = -\frac{\partial^2 U_{ij}(\boldsymbol{r})}{\partial r^\mu_i \partial r^\nu_i} = -\frac{\partial^2 U_{ij}(\boldsymbol{r})}{\partial r^\mu_j \partial r^\nu_j} \tag{26}$$

The self-interaction of an atom with its translated copies does not add to the Hessian, as this energy is translationally invariant. Splitting the Hessian into real and reciprocal components produces the expression for the real space second derivative

$$\frac{\partial^2 U^r_{ij}(\boldsymbol{r})}{\partial r^2_{ij}} = \frac{B_{ij}\alpha^{n+2}}{\Gamma\left(\frac{n}{2}\right)}\sum_{\boldsymbol{l}}\left\{4e^{-a^2} + \frac{2(n+1)\,e^{-a^2}}{a^2} + \frac{n(n+1)\Gamma\left(\frac{n}{2},a^2\right)}{a^{n+2}}\right\} \tag{27}$$

The reciprocal space second derivative is best calculated directly, using

$$\frac{\partial^2 U^f_{ij}(\boldsymbol{r})}{\partial r^\mu_i\, \mathrm{d}r^\nu_i} = \frac{-\pi^{3/2}B_{ij}}{2^{n-3}\Gamma\left(\frac{n}{2}\right)V}\sum_{\boldsymbol{k}\neq 0}\cos(\boldsymbol{k}\cdot\boldsymbol{r}_{ij})|\boldsymbol{k}|^{n-3}\boldsymbol{k}^\mu\boldsymbol{k}^\nu\,\Gamma\left(\frac{3-n}{2},b^2\right) \tag{28}$$

2.5. Errors. *2.5.1. Additive Potentials.* While both the real space and reciprocal space sums in the evaluation of the energy are convergent, they still include an infinite number of terms. Therefore, to practically evaluate each sum, cutoffs need to be employed beyond which the contributions of those interactions

DOI: 10.1021/acs.jctc.5b00093
J. Chem. Theory Comput. 2015, 11, 3684−3695

are ignored. Ignoring these long-range terms introduces an error into the calculation of energy, forces, and other molecular properties.

In order to estimate this error, it is first assumed that there is a uniform density of interactions beyond the cutoff distance. This allows the transformation of the discrete summation into a continuous integral in the same manner as in eq 2.[14b] Using this approximation, the error in the real space sum ϵ^r resulting from the real space cutoff r_c can be given as

$$\epsilon^r \sim \frac{2\pi\alpha^{n-3}\langle B_{ij}\rangle}{(3-n)V\Gamma\left(\frac{n}{2}\right)}\left[(\alpha r_c)^{3-n}\Gamma\left(\frac{n}{2},\alpha^2 r_c^2\right) - \Gamma\left(\frac{3}{2},\alpha^2 r_c^2\right)\right] \tag{29}$$

Here, $\langle B\rangle$ represents the sum of potential coefficients given as $\langle B_{ij}\rangle = \sum_{ij}|B_{ij}|$. The derivation of this formula is given in the Supporting Information. In a similar fashion, by integrating over the neglected reciprocal lattice vectors, the truncation error of the reciprocal space sum ϵ^f can be approximated as

$$\epsilon^f \sim \frac{2\alpha^n\langle B_{ij}\rangle}{\sqrt{\pi}n\Gamma\left(\frac{n}{2}\right)}\left[\left(\frac{k_c}{2\alpha}\right)^n\Gamma\left(\frac{3-n}{2},\frac{k_c^2}{4\alpha^2}\right) - \Gamma\left(\frac{3}{2},\frac{k_c^2}{4\alpha^2}\right)\right] \tag{30}$$

2.5.2. Potentials of Alternating Sign. These estimates of error are somewhat pessimistic in that they assume that the potential parameters B_{ij} are all of the same sign and thus the errors in the potential are all additive. In cases where the sign B_{ij} alternates, such as in the Coulomb potential, errors from each pairwise term in the sum can cancel, lowering the overall error. A more optimistic estimation of the errors can be made that accounts for this possible cancellation of errors. Assuming that the errors from each term are normally distributed allows an estimate of the error to be given based on the standard deviation of the error distribution.[13a] Here, the real space error can be approximated as

$$\epsilon^r = \frac{2^{1/4}\sqrt{\pi}\alpha^{n-3/2}\sqrt{\langle B_{ij}^2\rangle}}{\sqrt{V}\Gamma\left(\frac{n}{2}\right)}\sqrt{\Gamma\left(-\frac{1}{2},2\alpha^2 r_c^2\right)} \tag{31}$$

whereas the Fourier space truncation error can be given as

$$\epsilon_f = \frac{2\alpha^n\sqrt{\langle B_{ij}^2\rangle}}{\Gamma\left(\frac{n}{2}\right)\sqrt{k_c^3 V}}\, e^{-k_c^2/4\alpha^2} \tag{32}$$

A derivation of each of these equations is also given in the Supporting Information. Here, $\langle B_{ij}^2\rangle$ represents the sum of the squares of the potential parameters, such that $\langle B_{ij}^2\rangle = \sum_{ij} B_{ij}^2$. In the case of a geometric potential, such as the Coulomb potential, this simplifies to $\langle B_{ij}^2\rangle = \langle B_{ii}\rangle^2 = (\sum_i B_{ii})^2$.

To gain some insight into how these error estimates work in practice, the estimated Coulomb potential errors in a unit cell of NaCl have been calculated for several different cutoffs. These are shown in Figure 1. Here, it is assumed that each atom bears a single ionic charge. These calculations show that new error estimates derived here follow closely those already given.[13a,14b] This can be seen in the general overlap of the Karasawa and additive error estimates as well as the overlap of the Kolafa and alternate estimates. The only exception is in the real space error estimates at short cutoff distances, where the approximation of the integrals used to derive the expressions begins to break down. This comparison also shows that allowing for the cancellation of terms in cases of alternating attractive and repulsive potentials lowers the estimated energy by an order of magnitude.

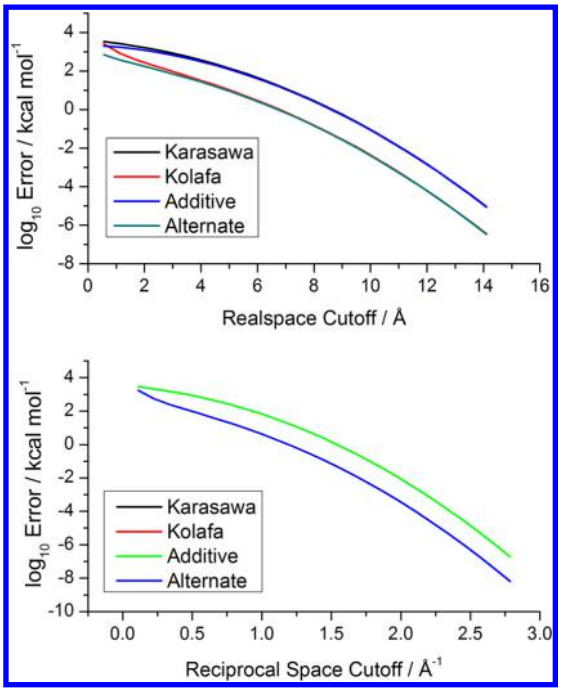

Figure 1. Real space and reciprocal space error estimates for NaCl. Karasawa and additive error estimates overlap, as do the Kolafa and alternate estimates.

2.6. Selection of the Convergence Parameter. In order to rapidly evaluate the Ewald sums, the convergence parameter α needs to be chosen carefully. The optimum strategy is to select α so that the real and reciprocal space sums take equivalent computational effort. It has been shown that selecting α in this way can reduce the scaling of the energy evaluation to $N^{3/2}$.[23] The computational effort required for each sum can be simply estimated by calculating the number of terms included within the cutoff limits, assuming a uniform density of terms. A scale factor that depends on the power of the potential χ_n may also be included, which reflects the ratio of the time taken for a single real and reciprocal space term. As shown by Karasawa and Goddard,[14b] the time needed for the real space and reciprocal space sums, τ_n^r and τ_n^f, respectively, can be given, therefore, as

$$\tau_n^r = \chi_n\frac{4\pi r_c^3 T}{3V} \tag{33}$$

and

$$\tau_n^f = \frac{k_c^3 VT}{12\pi^2} \tag{34}$$

Here, T represents the number of pairwise terms in the system. In the case where the reciprocal space sum is represented as in eq 14, the number of pairwise terms can be replaced with the number of atoms in the system.

While eq 33 gives a reasonable estimate of the computational effort for each sum, one complication is that while all the reciprocal space terms outside the cutoff radius can be eliminated at the start of the calculation, the real space terms cannot. Thus, the real space sum includes the time taken to scan over all possible translation vectors to find the terms

DOI: 10.1021/acs.jctc.5b00093
J. Chem. Theory Comput. 2015, 11, 3684−3695

within the cutoff radius. A better estimation of the real space summation time can be given, therefore, as

$$\tau_n^r = \chi_n \frac{4\pi r_c^3 T}{3V} + \psi T\left(L - \frac{4\pi r_c^3}{3V}\right) \tag{35}$$

Here, L represents the total number of translation vectors included in the cutoff radius and ψ is another scaling factor that sets the relative time of considering a real space term outside the cutoff radius with the time taken for a reciprocal space term.

The values of the scale factors χ_n and ψ will depend on the specific details of the implementation of the Ewald summation, including possible vectorization of the necessary function evaluations. They can be set empirically from calculations performed on model systems. As a guide, in our implementation of Ewald summation, we use values of 1.5, 1.0, and 2.0 for χ_1, χ_6, and χ_{12}, respectively. The need to consider additional translation vectors beyond the minimum image in the real space sum adds additional complexity in optimizing the Ewald sum. This introduces a discontinuity in the estimates of real space time as the cutoff radius crosses over the unit cell boundary. The effect of scanning over additional translation vectors can also be minimized by comparing squares of distances rather than the distances themselves, avoiding expensive square root function evaluations. In the following calculations, a value of 0 was used for ψ, effectively ignoring this term. This has had minimal impact on the efficiency of our calculations, as, in most cases, the optimal real space cutoff was less than half of the unit cell length. In calculations using smaller unit cells, this term may become significant, and greater efficiency may be achieved through a nonzero value of ψ.

3. OPTIMIZATIONS OF EWALD CALCULATIONS

3.1. Optimization of the Reciprocal Sum. GCMC simulations provide both some challenges and opportunities for optimizing the calculation of nonbonding interactions with Ewald summation. One advantage in GCMC simulations is that, unlike EMD simulations, typically only a small number of gas atoms move between energy evaluations as gases are moved one at a time. This means that during each energy evaluation only the interactions with the moving atoms need to be considered. Another advantage is that in GCMC simulations only the single energy change resulting from the proposed move is required. Forces for each atom do not need to be calculated.

These advantages lead to some important general optimizations. Since the framework atoms are considered to be static, the interactions between the gas and the framework can be precomputed and simply looked up for each energy evaluation.[39] This removes the scaling of the calculations with the size of the framework. Another advantage of this technique is that, while GCMC simulations are, in general, difficult to parallelize, the calculation of gas−framework interactions across a three-dimensional grid is not. Thus, these grids can be relatively quickly calculated using parallel programs.

The mainly static nature of the energy calculation can also be exploited in the representation of the reciprocal space energy sum between gas molecules. Similar to eq 8, in GCMC simulations, this sum can be represented as

$$U_n^f = \sum_{i\in X}\sum_{j\in Y} B_{ij} \sum_{\boldsymbol{k}\neq 0} [F_n(\boldsymbol{k}) \cos(\boldsymbol{k}\cdot\boldsymbol{r}_{ij})] \tag{36}$$

Here, $F_n(\boldsymbol{k})$ is a factor that depends on the reciprocal vector and also the order of the potential and is given as

$$F_n(\boldsymbol{k}) = \frac{\pi^{3/2}|\boldsymbol{k}|^{n-3}}{2^{n-2}\Gamma\left(\frac{n}{2}\right)V}\Gamma\left(\frac{3-n}{2}, \frac{|\boldsymbol{k}|^2}{4\alpha^2}\right) \tag{37}$$

In cases where the potential parameter B_{ij} obeys eq 13, then this sum can be rewritten as

$$U_n^f = \sum_{\boldsymbol{k}\neq 0} F_n(\boldsymbol{k})[(\sum_{j\in X\cup Y} \sqrt{B_{jj}}\, e^{i\boldsymbol{k}\cdot\boldsymbol{r}_j})^\dagger - (\sum_{j\in X} \sqrt{B_{jj}}\, e^{i\boldsymbol{k}\cdot\boldsymbol{r}_j})^\dagger - (\sum_{j\in Y} \sqrt{B_{jj}}\, e^{i\boldsymbol{k}\cdot\boldsymbol{r}_j})^\dagger] \tag{38}$$

Here, the symbol † represents the conjugate square of the imaginary sum. X is the set of trial gas atoms, and Y is the set of the remaining gas atoms. A similar expression can also be constructed for cases that do not use a geometric expression for B_{ij} by grouping the values of B_{ij} as in eq 16. Evaluated fully at each step, this representation of the energy is not much of an improvement; however, if the sums used for each set of atoms are retained in memory for each reciprocal vector between calculations, then this sum can be sped up significantly.[30] Utilizing the complete sum of all the atoms from the previous step S_k, the reciprocal energy of moving a gas from position X to Y can be given as

$$U_n^f = \sum_{\boldsymbol{k}\neq 0} F_n(\boldsymbol{k})[(S_k - \sum_{j\in X} \sqrt{B_{jj}}\, e^{i\boldsymbol{k}\cdot\boldsymbol{r}_j} + \sum_{j\in Y} \sqrt{B_{jj}}\, e^{i\boldsymbol{k}\cdot\boldsymbol{r}_j})^\dagger - (S_k - \sum_{j\in X} \sqrt{B_{jj}}\, e^{i\boldsymbol{k}\cdot\boldsymbol{r}_j})^\dagger - (\sum_{j\in Y} \sqrt{B_{jj}}\, e^{i\boldsymbol{k}\cdot\boldsymbol{r}_j})^\dagger] \tag{39}$$

S_k is updated after every successful Monte Carlo step, removing the contribution from the previous gas position and adding in the contribution from the new gas position. Since the sums in eq 39 are over only a set of single gas atoms, this effectively removes the scaling of the calculation of the reciprocal Ewald sum with the number of gas molecules in the system. For systems that have many gas molecules, this can lead to a large reduction in the size of the reciprocal sum. The estimation of the time taken for this reciprocal sum can be given as

$$\tau_n^f = \frac{k_c^3 V N_g}{12\pi^2} \tag{40}$$

Here, N_g represents the average number of gas atoms.

For Monte Carlo simulations that use atomic force or for EMD simulations with frozen atoms, a similar technique can be used to accelerate the evaluation of atomic forces. Dividing the atoms into a set of frozen atoms X and a set of mobile atoms Y, the total sum of terms for a reciprocal vector R_k can be given as

$$R_k = \sum_{j\in X} \sqrt{B_{jj}}\, e^{i\boldsymbol{k}\cdot\boldsymbol{r}_j} + \sum_{j\in Y} \sqrt{B_{jj}}\, e^{i\boldsymbol{k}\cdot\boldsymbol{r}_j} \tag{41}$$

The reciprocal space force on each atom f_j^f is then given as

$$f_j^f = \sum_{\boldsymbol{k}\neq 0} \sqrt{B_{jj}} F_n(\boldsymbol{k})\boldsymbol{k}[i\, e^{-i\boldsymbol{k}\cdot\boldsymbol{r}_j} R_k - i\, e^{i\boldsymbol{k}\cdot\boldsymbol{r}_j} R_k^*] \tag{42}$$

Here, R_k^* is used to signify the complex conjugate of the imaginary sum. To accelerate the evaluation of the forces, the sum R_k can be retained in memory. For Monte Carlo simulations, it can be advantageous to save the entire sum

DOI: 10.1021/acs.jctc.5b00093
J. Chem. Theory Comput. 2015, 11, 3684−3695

and update it for each successful move in a similar way as that for the calculation of energies. In EMD simulations, only the first part of the sum over frozen atoms needs to be retained, as the second part of the sum is recalculated at every step.

As mentioned previously, improving the efficiency of GCMC simulations presents both opportunities and challenges. The main challenge in optimizing GCMC simulation efficiency is that the number of gas molecules in the system, and thus the effort required for each energy evaluation, is an output of the calculation. This means that at the start of the simulation it is difficult to determine optimal parameters for the energy evaluation. This is particularly true if a constant truncation error is to be used in the simulations. As can be seen from the estimations of truncation error, the size of the error is dependent on the density of interactions within the simulation cell. Thus, for a given set of Ewald parameters, as more gas loads into the system the evaluation of the energies becomes increasingly less precise. To maintain the same truncation errors, the cutoffs need to be increased with the number of gas molecules.

While the size of the real space sum scales with both the cutoff and the number of gas molecules, using eq 39 the reciprocal sum only scales with the cutoff radius. Thus, to maintain an optimal calculation of the Ewald sums, it is advantageous to change the convergence parameter α and the corresponding cutoffs so as to increase the relative size of the reciprocal sum and decrease the real space sum so that the two remain in proportion. This also has the advantage of ensuring that the sums are evaluated to a constant accuracy throughout the calculation. This can also be used to limit the effect of truncation in the van der Waals potential, by equating the cutoff truncation error in the dispersion and repulsion potentials, so that the two errors cancel. Appropriate parameters can be automatically found for a specified truncation error through iteratively varying α until an optimum balance can be found. The balance of the sums can be checked periodically every certain number of steps, or it can be changed in response to changes in the average gas loading in the system.

3.2. Grid-Based Approximations. Another method for accelerating the Ewald sum has been recently discussed by Kim and Smit.[39b] In this method, grid points are used to precalculate the cosine terms in eq 36 over the reciprocal vectors. The value of the reciprocal energy for any pair interaction $\boldsymbol{r}_{ij}$ is then looked up on the grid instead of being directly calculated. This removes the scaling of the reciprocal sum with the cutoff but retains the scaling with the number of gas interactions in the system.

This method presents several challenges. Most notable is both the large memory and computational requirements in constructing the reciprocal term grid. While a single grid may be used for all of the potential interactions and for several pressure points, it is still far from computationally trivial to create the grid. This also poses problems in assigning optimal Ewald summation parameters, as it is too inefficient to re-evaluate the parameters in response to gas loading and therefore recalculate the grid. Parameters must be fixed at the start of the simulation without knowledge of the likely gas loading and number of interaction terms. This also means that the overall accuracy of the truncation of the Ewald sums is also uncertain.

The memory requirements for this method are also substantial. Typically, a small grid spacing, of the order of 0.2 Å or less, needs to be used to obtain reasonable accuracy. Using large simulation cells, this leads to grids that may require gigabytes of RAM. While they neglect to give the precise grid spacing used in their calculations, Kim and Smit do note that the Ewald grid for the Coulomb interactions does not fit into the 3 GB of their GPU processors. When using more traditional parallelization schemes, such as the single program multiple data (SPMD) scheme implemented in MPI to effectively parallelize the reciprocal space calculation, the grid needs to be replicated across the nodes, increasing the required memory for the calculation.

The methodology for setting optimal Ewald parameters for this scheme is also not obvious. Since the scaling of the reciprocal sum does not depend on the cutoff, one possible method would be to set the convergence parameter α so as to eliminate the real space sum, resulting in the entire sum being carried out in reciprocal space. The problem with this is that it often leads to such a large number of reciprocal vectors that the initial calculation of the grid becomes intractable. A more reasonable solution would be to set α such that the real and reciprocal space sums take roughly equivalent time. Given that in this scheme the time for the reciprocal space sum is simply the product of the number of terms in cell and the grid reading time, then, using eq 33, the real space cutoff required can be estimated as

$$r_c \approx \sqrt[3]{\frac{3G_n V}{4\pi}} \tag{43}$$

Here, G_n represents the ratio between the time taken for a grid read and a real space evaluation. Assuming a best case where $G_n \approx 1$, then the real space cutoff approaches half of the cell length. Therefore, it is proposed that one reasonable method for setting the Ewald parameters would be to set the real space cutoff using the minimum image convention. Then, α and k_c can be set to provide truncations of the real and reciprocal space sums to a certain accuracy based on an estimation of the maximum loading of the material. That would ensure both that the Ewald sums remain accurate during the simulation and that there is a reasonable balance between the real and reciprocal space sums. This is the approach taken in the simulations in this article.

3.3. Neglecting the Reciprocal Space Sum. Another approach that has been suggested is that of partially or completely ignoring the reciprocal space sum and including only the real space sum and the self-interaction energies in the final calculation.[29] Although it may result in a much faster calculation, it raises serious concerns about the accuracy of the simulation. This is especially true in cases where there are strong interactions, such as the electrostatic potential between water molecules. It also presents challenges in setting the Ewald parameters, as there is no simple way to estimate the systematic effect of neglecting the reciprocal sum for different values of the convergence parameter α. In general, it would seem far more advantageous, rather than neglecting the reciprocal sum, to simply abandon Ewald summation and use instead a complete pairwise potential, such as the shifted-force potential.[27a] These approximations take a similar amount of time as that for the real space component of the Ewald sum, and the errors associated with them are more controllable. Due to the concerns raised about neglecting the reciprocal space sum, this method is not further analyzed in our simulations.

DOI: 10.1021/acs.jctc.5b00093
J. Chem. Theory Comput. 2015, 11, 3684−3695

4. EXAMPLE SIMULATIONS

4.1. Computational Method. To illustrate and compare some of the possible methods for treating nonbonding interactions in GCMC and EMD simulations, a series of simulations of the adsorption and diffusion of CO_2 into the MOF material, MOF-5 (IRMOF-1),[40] has been performed. This MOF has been widely studied both experimentally and computationally for its gas adsorption and gas transport properties.[41] Since MOF-5 is a typical MOF material, these simulations will give some insight into the performance of the various treatments of nonbonding interactions in this class of materials.

In these simulations, five different methods for calculating the electrostatic and van der Waals potentials have been used. In the first scheme, the nonbonding interactions were calculated using the accelerated Ewald scheme discussed in eq 39 for the energies and eq 42 for the forces. To evaluate the relative speed increase with this method, a second Ewald-based method was employed using the representations of the reciprocal sum in eqs 36. In the third method, the reciprocal sum was calculated using the grid-based method. Finally, in the fourth and fifth methods, the potentials were calculated using shifted force[27a] (SF) and shifted force gradient[27b] (SFG) potentials of the general forms

$$U_n(r) = B_{ij}\left\{\frac{\mathrm{erfc}(\alpha r)}{r^n} - \frac{\mathrm{erfc}(\alpha r)}{r_c^n} + \left[n\frac{\mathrm{erfc}(\alpha r_c)}{r_c^{n+1}} + \frac{2\alpha e^{-\alpha^2 r_c^2}}{\sqrt{\pi} r_c^n}\right](r - r_c)\right\} \quad (44)$$

for the SF potential and

$$U_n(r) = B_{ij}\left\{\frac{1}{r^n} - \frac{1}{r_c^n} + \frac{n(r - r_c)}{r_c^{n+1}} - \frac{n(n+1)(r - r_c)^2}{2r_c^{n+2}}\right\} \quad (45)$$

for the SFG potential. Potentials of these types have been used in a number of simulations of gas adsorption in MOFs[42] and zeolites[43] and therefore form a reasonable comparison to Ewald methods.

In order to create meaningful comparisons the Ewald parameters, the first two methods were optimized during the simulation to attempt to find the best scaling properties and performance. The parameters for the grid-based method were set using the minimum image real space cutoff. The SF and SFG potentials all used a cutoff of 20 Å. A damping factor of 0.2 $Å^{-1}$ was used for the electrostatic SF potential, whereas other SF and SFG potentials were undamped. All gas−gas Ewald summations were performed to a truncation error of 10^{-3} kcal mol^{-1}, whereas the gas−framework interactions, where separated from the gas−gas interactions, were summed to an error of 10^{-5} kcal mol^{-1}.

The GCMC simulations were carried out using an in-house GCMC program. In each simulation, 10^6 equilibration and 10^7 production cycles were used. Insertion, deletion, rotation, translation, and reposition moves were used. A cavity-biased Monte Carlo method[44] was used to accelerate the convergence of the calculation, with up to 1000 trial molecules used for each insertion. The structure of MOF-5 was taken from the literature.[40] The van der Waals potentials for the framework atoms were taken from the Universal force field,[35] and the atomic charges were assigned according to the recent CBAC method.[45] The van der Waals parameters and charges for CO_2 were taken from the TraPPE force field.[36b] Interactions between gas and framework atoms were precalculated on a grid of points with a spacing of 0.15 Å. For comparison of the scaling of the calculation, simulations using both the original unit cell and a 2 × 2 × 2 supercell of the material were carried out. All simulations were performed at 298 K.

As with the GCMC simulations, the EMD simulations were performed using code developed within our group. Here, the same van der Waals and electrostatic potentials as in the GCMC simulations were used. A 2 × 2 × 2 supercell of the unit cell was used for the simulation cell. The framework atoms in each simulation were considered to be fixed during the simulation, with gas−framework interactions calculated at each step. In the EMD simulations, a time step of 1 fs was used. Each calculation was equilibrated by first performing a 1 ns simulation in the NVT ensemble at 298 K using the Nosé−Hoover thermostat,[46] followed by a further 1 ns simulation using the NVE ensemble. Mean-squared displacements and self-diffusion coefficients were calculated using a trajectory of 2 ps per gas molecule. Gas positions were recorded every 0.5 ps. Errors in the self-diffusion coefficient were estimated by breaking the trajectory into 20 independent segments and calculating the standard error.

4.2. GCMC Simulations. *4.2.1. CO_2 Loading.* Using the 5 methods outlined in the previous section, the loading of CO_2 in MOF-5 was calculated at 16 pressure points spaced logarithmically between 0.1 and 50 bar. To illustrate the effect of the gas−framework and gas−gas interactions, another simulation using Ewald summation for the gas−framework interactions and the SF potential for the gas−gas interactions is also included. This method is referred to as the SF/Ewald method. As would be expected, the methods that use the atom-, pair-, and grid-based reciprocal sums produce similar adsorptions, as they are essentially numerically equivalent. The loading calculated from the Ewald method, the SF method, the SFG method, and the hybrid SF/Ewald method is compared in Figure 2 with the experimentally determined loading.[41]

Here, we see that each of the pair-based potentials produces a lower adsorption to the Ewald method. This difference is most pronounced in the range of 5−20 bar. The percentage differences between the Ewald and pair potentials adsorptions at 9.5 bar is 18% for the SF potential, 25% for the SFG

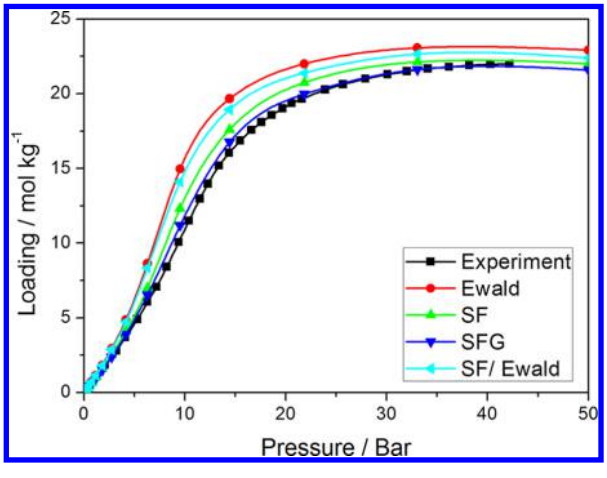

Figure 2. Simulated and experimental loading of CO_2 in MOF-5.

DOI: 10.1021/acs.jctc.5b00093
J. Chem. Theory Comput. 2015, 11, 3684−3695

potential, and 5% for the SF/Ewald potential. While the pair potentials, particularly the SFG potential, are closer to the experimental adsorption, this is due to a cancellation of errors in the Univeral/TraPPE/CBAC force field and the potential summation method. The much smaller discrepancy between the Ewald and SF/Ewald isotherms shows that most of the error in the SF and SFG isotherms is likely due to gas−framework interactions. However, at intermediate to higher loading, as the density of gas molecules in the pore increases, the gas−gas interactions also become significant. The difference between these methods may also increase for more polar gases, such as water, where the overall dipole moment increases the electrostatic interactions between molecules.

To further understand the discrepancies between each method, the average total van der Waals, electrostatic, and total energy per gas molecule is shown in Figure 3. First,

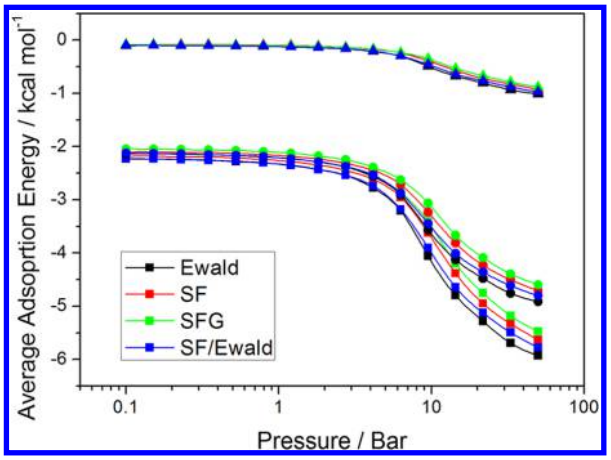

Figure 3. Average van der Waals (circles), electrostatic (triangles), and total (squares) adsorption energy components.

looking at the van der Waals energies, it can be seen that even at low pressure the SF and SFG adsorption energies are slightly higher than the Ewald and the SF/Ewald energies. This difference increases at higher pressure as the gas−gas interactions become important and adsorption energy is lowered. The significance of the gas−gas interactions can also be seen in the divergence of the Ewald and SF/Ewald methods. As the Ewald energy is lower, the discrepancy is most likely due to the nonconvergence of the dispersion potential. This is in spite of relatively long 20 Å cutoffs being used in each case. This result highlights the benefit of higher accuracy in applying Ewald summation to dispersion potentials. Interestingly, in contrast to the dispersion potentials, the electrostatic potential is almost identical at low pressure, diverging only slightly at high pressure. Due to the general nonconvergence of this potential, it might be expected that this energy would show the most difference between the pair-potential and Ewald based methods. However, it appears that the quadrupolar nature of CO_2 electrostatic potential can be accurately estimated with pair-based potentials. There is also little difference here between the damped SF potential and the undamped SFG potential.

4.2.2. Simulation Timing. To determine the relative timings for each simulation, the wall time taken by the routines that calculate the gas−gas interaction potentials was recorded during the simulation. These were then summed to provide an overall time spent in evaluating the energy in each simulation. Using this method, the time taken for the Monte Carlo routines is not included, allowing a direct comparison between the timings of different energy evaluation methods. In the code, the internal energy evaluation loops are parallelized with MPI during the equilibration phase. During the production phase, independent sampling was carried out on each CPU. As the production phase uses an order of magnitude more steps than the equilibration, the results of these calculations are largely unaffected by the efficiency of the parallelization.

The results of these calculations are shown in Figure 4. Here, timings are shown both for the 1 × 1 × 1 and 2 × 2 × 2

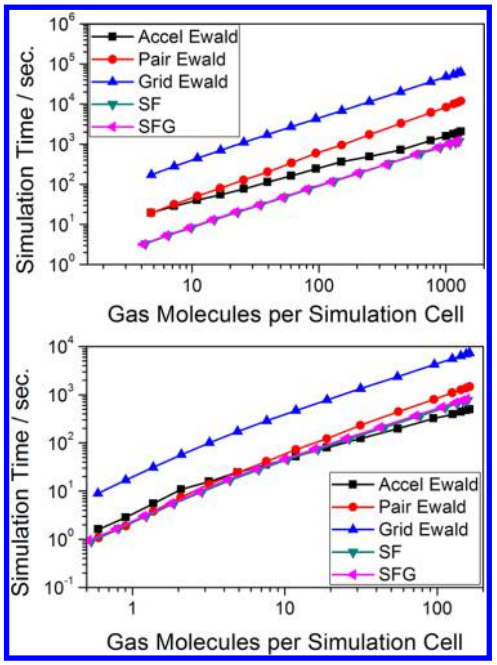

Figure 4. Calculation wall time for different energy evaluation algorithms in the 2 × 2 × 2 simulation cell (top) and the 1 × 1 × 1 simulation cell (bottom).

simulation cells. All of these calculations show the expected linear dependence between simulation size and time, with the exception of the accelerated Ewald method. This method scales in a sublinear manner. This is a result of shifting the convergence parameter during the simulation to place more work on the nonlinear scaling reciprocal space sum. While in the larger 2 × 2 × 2 simulation cell the overall the SF and SFG potentials are the fastest methods for calculating the gas−gas interactions, in the smaller 1 × 1 × 1 cell the accelerated Ewald method takes less time than the SF and SFG potentials at high loading. This is due to the cutoffs used in the SF and SFG potentials extending beyond the minimum image terms, while at higher loading the Ewald method uses a shorter cutoff and therefore includes only the minimum image terms. The pairwise-based Ewald methods show similar performance to the accelerated Ewald method at low loading, but they show poor performance at higher pressure as the increased number of gas−gas interactions significantly slows the evaluation of the reciprocal space sum.

To better illustrate the nonlinear scaling of the accelerated Ewald method, the ratio between the shifted force and accelerated Ewald method energy evaluation times is shown in Figure 5, along with the real space cutoff radius used in each

DOI: 10.1021/acs.jctc.5b00093
J. Chem. Theory Comput. 2015, 11, 3684−3695

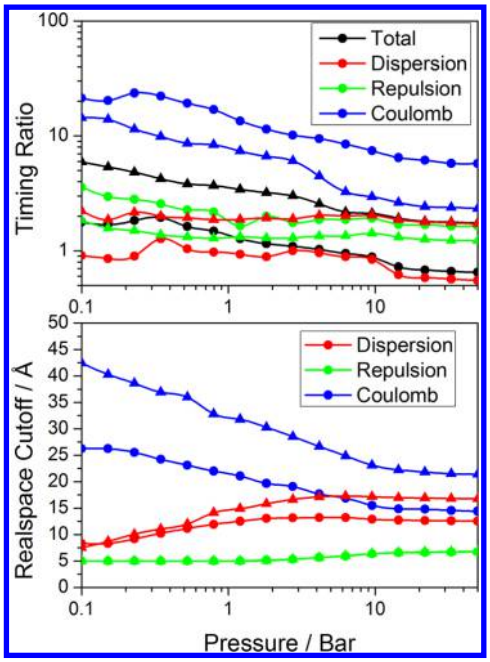

Figure 5. Timing ratio and optimal real space cutoffs for accelerated Ewald in 1 × 1 × 1 (circles) and 2 × 2 × 2 (triangles) simulation cells.

Ewald calculation. Data for both the 1 × 1 × 1 and 2 × 2 × 2 simulation cells is shown. As can be seen here, as the pressure, and therefore the number of molecules in the system, is increased, the ratio between the accelerated Ewald summation and shifted force summation approaches 0.6 for the 1 × 1 × 1 simulation and 1.75 for the 2 × 2 × 2 simulation. It should be noted that these timings do not include the rest of the simulation timing, particularly the time taken in preselection of gas position. Taking into account the total wall time at high pressure, the ratio between the Ewald and SF methods is 1.1 for the 1 × 1 × 1 simulation and 1.3 for the 2 × 2 × 2 simulation. Here, the reason for the increase in time for the Ewald summation in the 1 × 1 × 1 cell is due to the slightly higher CO_2 density in this simulation and the calculation time taken by the cavity finding algorithm, which is comparatively much larger in the Ewald case. This change illustrates that at large pressure the difference in time between Ewald and pair-based methods becomes negligible, as other factors start to have a significant impact on the efficiency of the calculation.

At higher pressure ranges, the material begins to become saturated and therefore the timing for both methods becomes constant with increasing pressure. Interestingly, looking at the change in the cutoff radius, it can be seen that while the Coulomb potential cutoff is decreased at higher pressure in response to more calculation being done in reciprocal space, the dispersion and repulsion cutoffs increase in response to the need to maintain the same error limits at higher density. This demonstrates that it is primarily the electrostatic interactions that are responsible for the nonlinear scaling of this method.

The most surprising result is the very poor performance of the grid-based Ewald method. This shows significantly worse performance than any other Ewald method, even simply directly calculating the same sum. This is surprising given that in other studies this method has been shown to be significantly faster than other Ewald summation techniques.[39b] In our calculations, we have been careful to provide the parameters that optimize each sum so as not to give a false impression of the relative speeds of the different methods. Therefore, in the reciprocal pair-based method, real space cutoffs of up to 66 Å were used to balance reciprocal space cutoffs of only approximately 0.4 $Å^{-1}$ in the electrostatic sums. This shows that for optimal Ewald parameters there is simply not enough computation done on the reciprocal space sum to justify the expensive grid interpolation operation. In their study on efficient Monte Carlo simulation, Kim and Smit used a larger set of reciprocal space vectors, which may explain the sizable speedup in going from a pair-based to a grid-based Ewald method.[39b]

It should also be noted that the performance of the grid-based Ewald method is based on the particular implementation of this method. Since this method relies on fast memory access, then the specific details of the simulation cell, grid size, and computer hardware become important. It is difficult to make meaningful timing comparisons between methods, as grid-based Ewald is memory-bound, whereas others are CPU-bound. In general, it appears that grid-based Ewald summation is not competitive with well-optimized accelerated Ewald schemes. This is especially highlighted by the poor performance of the grid-based method in both the 1 × 1 × 1 and 2 × 2 × 2 simulations.

4.3. Molecular Dynamics Simulations. To test the applicability of the Ewald and pair potential methods in a different type of simulation, the self-diffusion coefficient of CO_2 in MOF-5 has been calculated using EMD simulations for a range of CO_2 loadings. Both diffusion and adsorption of gases are largely influenced by different regions of the potential energy surface. While adsorption is mostly determined by the strength of binding to low-energy adsorption sites, diffusion is strongly influenced by the energy barriers between adsorption sites. In these simulations, only the accelerated Ewald, SF, and SFG potentials were used, as the other Ewald based methods should provide similar results as those with the accelerated Ewald method. The calculated self-diffusion coefficients with their respective errors are shown in Figure 6.

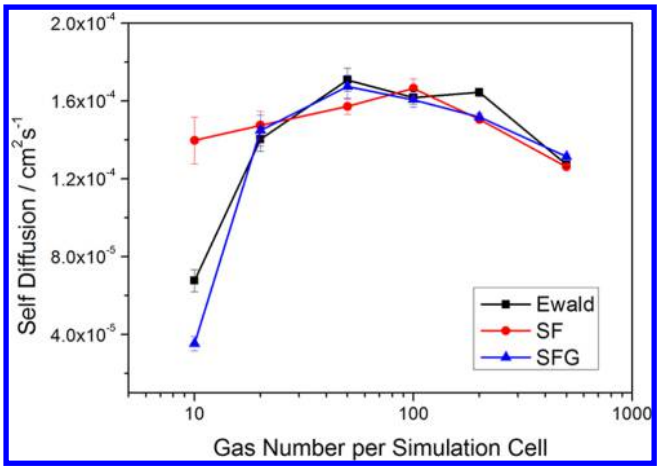

Figure 6. Self-diffusion coefficients of CO_2 in MOF-5 at 298 K.

First, it can be seen that the calculated self-diffusion coefficients are in good agreement with others previously calculated.[41b] At higher pressures, there is no consistent difference between the diffusion coefficients calculated with the Ewald and pair potential methods. At the lowest gas loading of 10 CO_2 molecules per simulation cell, there does appear to

DOI: 10.1021/acs.jctc.5b00093
J. Chem. Theory Comput. 2015, 11, 3684−3695

be a significant difference between the SF potential, which uses damped electrostatics, and the Ewald and SFG potential that uses undamped electrostatics. In the case of low gas loading, the precise interactions between the gas and the framework, including potential adsorption sites, become more significant. This may account for some of the difference between these diffusion measurements. According to the previous adsorption simulations, a gas loading of 10 CO_2 molecules per simulation cell corresponds to a total pressure of approximately 20 kPa, so this is mostly a problem in calculating the diffusion of rarefied gases.

5. CONCLUSIONS

In this article, we have shown how Ewald summation can be applied to a number of simulation types and potentials. While typically slower than simpler pair potential-based methods, Ewald summation offers greater control over the accuracy of the calculation. This article also shows that in Monte Carlo simulations it is possible to optimize the calculation of energies so as to have both high accuracy and a similar computational cost to that of pair-based methods. Here, directly reusing the results of previous energy calculations and intelligently setting the convergence parameter is shown to be much faster than other similar optimizations using lookup grids. Correctly balancing the real and reciprocal space sums allows for a sublinear scaling that is especially suited to calculations of adsorption at high pressure. Ewald summation is also shown to be useful in the calculation of both electrostatic and dispersion potentials, as simple pair-based methods do not fully converge, even with typically long cutoffs. Given their similar computational cost and increased accuracy, Ewald methods should be considered as a default method of calculation for both electrostatic and van der Waals interactions in Monte Carlo simulations.

In the case of molecular dynamics simulations of gas diffusion, these were shown to be less sensitive to the method used to calculate the atomic forces, showing significant differences between methods only at low pressures. The application of direct Ewald summation is also limited to calculations that have a large number of fixed atoms. In calculations of gas diffusion, where the motion of the framework plays a significant role in diffusion,[47] this method may not be effective. In these cases, pair-based potentials or other formulations of the Ewald method, such as smoothed particle mesh Ewald, may be more efficient.

■ ASSOCIATED CONTENT

Supporting Information

The Supporting Information is available free of charge on the ACS Publications website at DOI: 10.1021/acs.jctc.5b00093.

Derivation of both of the formulas for the Ewald energy as well as the resulting cutoff errors (PDF).

■ AUTHOR INFORMATION

Corresponding Authors

*E-mail: Brad.Wells@monash.edu (B.A.W).
*E-mail: Alan.Chaffee@monash.edu (A.L.C.).

Funding

The authors acknowledge the support provided by the Australian Government through its CRC Program for this CO2CRC research project.

Notes

The authors declare no competing financial interest.

■ ACKNOWLEDGMENTS

The authors would like to thank Dr. Tim Garoni for his helpful comments on the prepared manuscript.

■ REFERENCES

(1) (a) Frenkel, D.; Smit, B. Monte Carlo Simulations. *Understanding Molecular Simulation*, 2nd ed.; Academic Press: San Diego, CA, 2002; pp 23−61. (b) Frenkel, D.; Smit, B. Monte Carlo Simulations in Various Ensembles. *Understanding Molecular Simulation*, 2nd ed.; Academic Press: San Diego, CA, 2002; pp 111−137.

(2) (a) Frenkel, D.; Smit, B. Molecular Dynamics Simulations. *Understanding Molecular Simulation*, 2nd ed.; Academic Press: San Diego, CA, 2002; pp 63−107. (b) Frenkel, D.; Smit, B. Molecular Dynamics in Various Ensembles. *Understanding Molecular Simulation*, 2nd ed.; Academic Press: San Diego, CA, 2002; pp 139−163.

(3) (a) Smit, B.; Maesen, T. L. M. *Chem. Rev.* **2008**, *108*, 4125−4184. (b) Getman, R. B.; Bae, Y.-S.; Wilmer, C. E.; Snurr, R. Q. *Chem. Rev.* **2012**, *112*, 703−723. (c) Keskin, S.; Liu, J.; Rankin, R. B.; Johnson, J. K.; Sholl, D. S. *Ind. Eng. Chem. Res.* **2009**, *48*, 2355−2371.

(4) Suh, M. P.; Park, H. J.; Prasad, T. K.; Lim, D.-W. *Chem. Rev.* **2012**, *112*, 782−835.

(5) Sumida, K.; Rogow, D. L.; Mason, J. A.; McDonald, T. M.; Bloch, E. D.; Herm, Z. R.; Bae, T.-H.; Long, J. R. *Chem. Rev.* **2012**, *112*, 724−781.

(6) Eastman, P.; Pande, V. S. *J. Comput. Chem.* **2009**, *31*, 1268−1272.

(7) (a) Chung, Y. G.; Camp, J.; Haranczyk, M.; Sikora, B. J.; Bury, W.; Krungleviciute, V.; Yildirim, T.; Farha, O. K.; Sholl, D. S.; Snurr, R. Q. *Chem. Mater.* **2014**, *26*, 6185−6192. (b) Colon, Y. J.; Snurr, R. Q. *Chem. Soc. Rev.* **2014**, *43*, 5735−5749. (c) Colón, Y. J.; Fairen-Jimenez, D.; Wilmer, C. E.; Snurr, R. Q. *J. Phys. Chem. C* **2014**, *118*, 5383−5389. (d) Wilmer, C. E.; Leaf, M.; Lee, C. Y.; Farha, O. K.; Hauser, B. G.; Hupp, J. T.; Snurr, R. Q. *Nat. Chem.* **2011**, *4*, 83−89. (e) Lin, L.-C.; Berger, A. H.; Martin, R. L.; Kim, J.; Swisher, J. A.; Jariwala, K.; Rycroft, C. H.; Bhown, A. S.; Deem, M. W.; Haranczyk, M.; Smit, B. *Nat. Mater.* **2012**, *11*, 633−641. (f) Wilmer, C. E.; Farha, O. K.; Bae, Y.-S.; Hupp, J. T.; Snurr, R. Q. *Energy Environ. Sci.* **2012**, *5*, 9849−9856.

(8) (a) Rappe, A. K.; Casewit, C. J.; Colwell, K. S.; Goddard, W. A.; Skiff, W. M. *J. Am. Chem. Soc.* **1992**, *114*, 10024−10035. (b) Jorgensen, W. L.; Maxwell, D. S.; Tirado-Rives, J. *J. Am. Chem. Soc.* **1996**, *118*, 11225−11236. (c) Mayo, S. L.; Olafson, B. D.; Goddard, W. A. *J. Phys. Chem.* **1990**, *94*, 8897−8909.

(9) Verstraelen, T.; Ayers, P. W.; Van Speybroeck, V.; Waroquier, M. *J. Chem. Theory Comput.* **2013**, *9*, 2221−2225.

(10) Yang, Q.; Liu, D.; Zhong, C.; Li, J.-R. *Chem. Rev.* **2013**, *113*, 8261−323.

(11) Steinbach, P. J.; Brooks, B. R. *J. Comput. Chem.* **1994**, *15*, 667−683.

(12) Frenkel, D.; Smit, B. Long-Range Interactions. *Understanding Molecular Simulation*, 2nd ed.; Academic Press: San Diego, CA, 2002; pp 291−320.

(13) (a) Kolafa, J.; Perram, J. W. *Mol. Simul.* **1992**, *9*, 351−368. (b) Ewald, P. P. *Ann. Phys. (Berlin, Ger.)* **1921**, *369*, 253−287. (c) Toukmaji, A. Y.; Board, J. A., Jr *Comput. Phys. Commun.* **1996**, *95*, 73−92.

(14) (a) Chen, Z. M.; Çağin, T.; Goddard, W. A. *J. Comput. Chem.* **1997**, *18*, 1365−1370. (b) Karasawa, N.; Goddard, W. A. *J. Phys. Chem.* **1989**, *93*, 7320−7327. (c) Williams, D. E. *Acta Crystallogr., Sect. A: Cryst. Phys., Diffr., Theor. Gen. Crystallogr.* **1971**, *27*, 452−455.

(15) Aguado, A.; Madden, P. A. *J. Chem. Phys.* **2003**, *119*, 7471−7483.

(16) (a) Osychenko, O. N.; Astrakharchik, G. E.; Boronat, J. *Mol. Phys.* **2012**, *110*, 227−247. (b) Martial, M. *J. Phys. A: Math. Theor.* **2010**, *43*, 425002.

(17) Ballenegger, V.; Cerdà, J. J.; Holm, C. *J. Chem. Theory Comput.* **2012**, *8*, 936−947.
(18) Darden, T.; York, D.; Pedersen, L. *J. Chem. Phys.* **1993**, *98*, 10089−10092.
(19) Essmann, U.; Perera, L.; Berkowitz, M. L.; Darden, T.; Lee, H.; Pedersen, L. G. *J. Chem. Phys.* **1995**, *103*, 8577−8593.
(20) (a) Ballenegger, V.; Cerda, J. J.; Lenz, O.; Holm, C. *J. Chem. Phys.* **2008**, *128*, 034109−13. (b) Eastwood, J. W.; Hockney, R. W.; Lawrence, D. N. *Comput. Phys. Commun.* **1980**, *19*, 215−261.
(21) York, D.; Yang, W. *J. Chem. Phys.* **1994**, *101*, 3298−3300.
(22) (a) Wennberg, C. L.; Murtola, T.; Hess, B.; Lindahl, E. *J. Chem. Theory Comput.* **2013**, *9*, 3527−3537. (b) Isele-Holder, R. E.; Mitchell, W.; Ismail, A. E. *J. Chem. Phys.* **2012**, *137*, 174107−13.
(23) Jackson, R. A.; Catlow, C. R. A. *Mol. Simul.* **1988**, *1*, 207−224.
(24) Fukuda, I.; Nakamura, H. *Biophys. Rev.* **2012**, *4*, 161−170.
(25) Neumann, M. *Mol. Phys.* **1983**, *50*, 841−858.
(26) (a) Yonezawa, Y. *J. Chem. Phys.* **2012**, *136*, 244103. (b) Wolf, D.; Keblinski, P.; Phillpot, S. R.; Eggebrecht, J. *J. Chem. Phys.* **1999**, *110*, 8254−8282.
(27) (a) Fennell, C. J.; Gezelter, J. D. *J. Chem. Phys.* **2006**, *124*, 234104−12. (b) McCann, B. W.; Acevedo, O. *J. Chem. Theory Comput.* **2013**, *9*, 944−950.
(28) Wu, X.; Brooks, B. R. *J. Chem. Phys.* **2005**, *122*, 044107.
(29) Moreno-Razo, J. A.; Díaz-Herrera, E.; Klapp, S. H. L. *Mol. Phys.* **2006**, *104*, 2841−2854.
(30) Vlugt, T. J. H.; García-Pérez, E.; Dubbeldam, D.; Ban, S.; Calero, S. *J. Chem. Theory Comput.* **2008**, *4*, 1107−1118.
(31) Kolafa, J.; Moucka, F.; Nezbeda, I. *Collect. Czech. Chem. Commun.* **2008**, *73*, 481−IX.
(32) Elvira, V. H.; MacDowell, L. G. *J. Chem. Phys.* **2014**, *141*, 164108.
(33) Nijboer, B. R. A.; de Wette, F. W. *Physica* **1957**, *23*, 309−321.
(34) Sun, H. *J. Phys. Chem. B* **1998**, *102*, 7338−7364.
(35) Rappé, A. K.; Casewit, C. J.; Colwell, K. S.; Goddard, W. A.; Skiff, W. M. *J. Am. Chem. Soc.* **1992**, *114*, 10024−10035.
(36) (a) Martin, M. G.; Siepmann, J. I. *J. Phys. Chem. B* **1998**, *102*, 2569−2577. (b) Potoff, J. J.; Siepmann, J. I. *AIChE J.* **2001**, *47*, 1676−1682.
(37) (a) Moučka, F.; Rouha, M.; Nezbeda, I. *J. Chem. Phys.* **2007**, *126*, 224106. (b) Moučka, F.; Nezbeda, I.; Smith, W. R. *Mol. Simul.* **2013**, *39*, 1125−1134.
(38) Escobedo, F. A. *J. Chem. Phys.* **1998**, *108*, 8761−8772.
(39) (a) Watanabe, T.; Manz, T. A.; Sholl, D. S. *J. Phys. Chem. C* **2011**, *115*, 4824−4836. (b) Kim, J.; Smit, B. *J. Chem. Theory Comput.* **2012**, *8*, 2336−2343.
(40) Li, H.; Eddaoudi, M.; O'Keeffe, M.; Yaghi, O. M. *Nature* **1999**, *402*, 276−279.
(41) (a) Saha, D.; Bao, Z.; Jia, F.; Deng, S. *Environ. Sci. Technol.* **2010**, *44*, 1820−6. (b) Skoulidas, A. I.; Sholl, D. S. *J. Phys. Chem. B* **2005**, *109*, 15760−15768. (c) Zhao, Z.; Li, Z.; Lin, Y. S. *Ind. Eng. Chem. Res.* **2009**, *48*, 10015−10020. (d) Zhao, Z.; Ma, X.; Li, Z.; Lin, Y. S. *J. Membr. Sci.* **2011**, *382*, 82−90. (e) Guo, H.-c.; Shi, F.; Ma, Z.-f.; Liu, X.-q. *J. Phys. Chem. C* **2010**, *114*, 12158−12165. (f) Gomez, D. A.; Combariza, A. F.; Sastre, G. *Phys. Chem. Chem. Phys.* **2009**, *11*, 9250−9258. (g) Gallo, M.; Glossman-Mitnik, D. *J. Phys. Chem. C* **2009**, *113*, 6634−6642. (h) Belof, J. L.; Stern, A. C.; Space, B. *J. Phys. Chem. C* **2009**, *113*, 9316−9320. (i) Pianwanit, A.; Kritayakornupong, C.; Vongachariya, A.; Selphusit, N.; Ploymeerusmee, T.; Remsungnen, T.; Nuntasri, D.; Fritzsche, S.; Hannongbua, S. *Chem. Phys.* **2008**, *349*, 77−82. (j) Yang, Q.; Zhong, C. *J. Phys. Chem. B* **2006**, *110*, 17776−17783. (k) Greathouse, J. A.; Allendorf, M. D. *J. Am. Chem. Soc.* **2006**, *128*, 10678−10679. (l) Millward, A. R.; Yaghi, O. M. *J. Am. Chem. Soc.* **2005**, *127*, 17998−17999. (m) Eddaoudi, M.; Kim, J.; Rosi, N.; Vodak, D.; Wachter, J.; O'Keeffe, M.; Yaghi, O. M. *Science* **2002**, *295*, 469−472. (n) Thallapally, P. K.; Grate, J. W.; Motkuri, R. K. *Chem. Commun.* **2012**, *48*, 347−349. (o) Lu, C.-M.; Liu, J.; Xiao, K.; Harris, A. T. *Chem. Eng. J.* **2010**, *156*, 465−470. (p) Xiang, S.; Zhou, W.; Gallegos, J. M.; Liu, Y.; Chen, B. *J. Am. Chem. Soc.* **2009**, *131*, 12415−12419. (q) Britt, D.; Tranchemontagne, D.; Yaghi, O. M. *Proc. Natl. Acad. Sci. U. S. A.* **2008**, *105*, 11623−11627.
(42) (a) Forrest, K. A.; Pham, T.; McLaughlin, K.; Belof, J. L.; Stern, A. C.; Zaworotko, M. J.; Space, B. *J. Phys. Chem. C* **2012**, *116*, 15538−15549. (b) Wells, B.; Chaffee, A. *Adsorption* **2011**, *17*, 255−264. (c) Forrest, K. A.; Pham, T.; Hogan, A.; McLaughlin, K.; Tudor, B.; Nugent, P.; Burd, S. D.; Mullen, A.; Cioce, C. R.; Wojtas, L.; Zaworotko, M. J.; Space, B. *J. Phys. Chem. C* **2013**, *117*, 17687−17698. (d) Sarkisov, L. *J. Phys. Chem. C* **2012**, *116*, 3025−3033.
(43) Pham, T. D.; Xiong, R.; Sandler, S. I.; Lobo, R. F. *Microporous Mesoporous Mater.* **2014**, *185*, 157−166.
(44) (a) Snurr, R. Q.; Bell, A. T.; Theodorou, D. N. *J. Phys. Chem.* **1993**, *97*, 13742−13752. (b) Yau, D. H. L.; Liem, S. Y.; Chan, K. Y. *J. Chem. Phys.* **1994**, *101*, 7918−7924.
(45) Xu, Q.; Zhong, C. *J. Phys. Chem. C* **2010**, *114*, 5035−5042.
(46) Hoover, W. G. *Phys. Rev. A: At., Mol., Opt. Phys.* **1985**, *31*, 1695−1697.
(47) (a) Parkes, M. V.; Demir, H.; Teich-McGoldrick, S. L.; Sholl, D. S.; Greathouse, J. A.; Allendorf, M. D. *Microporous Mesoporous Mater.* **2014**, *194*, 190−199. (b) Gee, J. A.; Chung, J.; Nair, S.; Sholl, D. S. *J. Phys. Chem. C* **2013**, *117*, 3169−3176.

DOI: 10.1021/acs.jctc.5b00093
J. Chem. Theory Comput. 2015, 11, 3684−3695